REFERENCES

1. Abdel-Dayem HM, Scott AM, Macapinlac HA, El-Gazzar AH, Larson SM. Role of Tl-201 chloride and Tc-99m-sestamibi in tumor imaging. In: Freeman LM, ed. *Nuclear Medicine Annual* New York, NY: Raven Press; 1994:181–234.
2. El-Gazzar AH, Fernandez-Ulloa M, Silberstein EG. Thallium-201 as a tumor imaging agent: current status and future consideration. *Nucl Med Commun* 1993;14:96–99.
3. El-Gazzar AH, Malki A, Abdel-Dayem HM, et al. Role of Tl-201 in the diagnosis of solitary bone lesions. *Nucl Med Commun* 1989:477–485.
4. Waxman A, Ramanna L, Memsie L, Silberman A, Brennar J. Thallium scintigraphy in the differentiation of malignant from benign mass abnormalities of the breast [Abstract]. *J Nucl Med* 1990;31:767.
5. Waxman AD, Ramannah L, Memsie LD, et al. Thallium scintigraphy in the evaluation of mass abnormalities of the breast. *J Nucl Med* 1993;34:18–23.
6. Ramannah L, Waxman AD, Weiss A, Rosen G. Thallium-201 scan patterns in bone and soft tissue sarcoma [Abstract]. *J Nucl Med* 1992;33:843.
7. Kim KT, Black KL, Marcino D, et al. Thallium-201 SPECT imaging of brain tumors; methods and results. *J Nucl Med* 1990;19:965–969.
8. Kaplan WD, Takuovian T, Morris J, et al. Thallium-201 brain tumor imaging: a comparative study with pathologic correlation. *J Nucl Med* 1987;28:47–52.
9. Gruber MC, Hochberg FH. Editorial: systemic evalution of primary brain tumors. *J Nucl Med* 1990;31:969–971.
10. Sjoholm BA, Elmquist D, Rehncrona S, Rosen I, Salford L. Thallium-201 and SPECT distinguishes high-grade from low-grade gliomas [Abstract]. *J Nucl Med* 1992;33:868.
11. Kosuda S, Aoki S, Suzuki K, Nakamura O, Shidara N. Reevaluation of quantitative thallium-201 brain SPECT for brain tumors [Abstract]. *J Nucl Med* 1992;33:844.
12. Hoh CK, Khannas S, Harris GC, et al. Evaluation of brain tumor recurrence with Tl-201 SPECT studies: correlation with FDG PET and histological results [Abstract]. *J Nucl Med* 1992;33:867.
13. Ramannah L, Waxman AD, Binney G, Waxman S, Mirra J, Rosen G. Tl-201 scintigraphy in bone sarcoma: comparison with Ga-67 and Tc-99m-MDP in the evaluation of chemotherapeutic response. *J Nucl Med* 1990;31:567–571.
14. Caluser C, Macapinlac H, Meyers P, et al. The relationship between thallium uptake, blood flow and blood pool radioactivity in bone and soft tissue tumors. *Clin Nucl Med* 1992;17:565–571.
15. Kostakoglu L, David PM, Divgi CR, Botet J, Healy J, Larson SM. Correlation of the findings of thallium-201 chloride scans with those of other imaging modalities and histology following therapy in patients with bone and soft tissue sarcomas. *Eur J Nucl Med.* 1995;22:1232–1237.
16. Sehweil AM, Mckillop JH, Milroy R, et al. Mechanism of Tl-201 uptake in tumors. *Eur J Nucl Med* 1989;15:376–379.
17. Ando A, Ando I, Katayana M, et al. Biodistribution of Tl-201 in tumor bearing animals and inflammatory lesions induced animals. *Eur J Nucl Med* 1987;12:567–572.
18. Sehweil A, McKillop JH, Ziada G, Al-Sayed M, Abdel-Dayem HM, Omar YT. The optimum time for tumor imaging with thallium-201. *Eur J Nucl Med* 1988;13:527–529.
19. Kaplan WD, Southee ML, Annese MS, et al. Evaluating low and intermediate grade non-Hodgkin's lymphoma (NHL) with gallium-67 and thallium-201 imaging [Abstract]. *J Nucl Med* 1990;31:793.
20. Abdel-Dayem HM, DiFabrizio L, Bag R, Aras T, Turoglu HT, Kempf JS, Habbab N, Pescatore F, Sadik A, Kowalsky W. Evaluation of sequential thallium and gallium scans in AIDS patients. *J Nucl Med* 1996;37:1662–1667.
21. Abdel-Dayem HM, DiFabrizio L, Aras T, et al. Prospective evaluation of sequential thallium-201 chloride and gallium-67 citrate scans in AIDS patients [Abstract]. *J Nucl Med* 1993;34:172P.
22. Lee VW. AIDS-related Kaposi's sarcoma–findings in thallium-201 scintigraphy. *Am J Roentgenol* 1988;151:1233–1235.
23. Ganz WI, Nguyen TQ, Benedetto MP, et al. Use of early, late and SPECT thallium imaging in evaluating activity of soft tissue and bone tumors [Abstract]. *J Nucl Med* 1993;34:32P.
24. Ueda T, Kaszi Y, Yakisaka S, et al. Time sequential single-photon emission computed tomography studies in brain tumor using thallium-201. *Eur J Nucl Med* 1993;20:138.
25. Chen DCP, Ma GQ, Ansari A, et al. Optimal imaging time for thallium as a tumor agent in patients with lymphoma [Abstract]. *J Nucl Med* 1992;33(suppl):44P.

PET 2-Fluoro-2-Deoxyglucose Uptake in Rat Prostate Adenocarcinoma During Chemotherapy with Gemcitabine

Uwe Haberkorn, Matthias E. Bellemann, Annette Altmann, Ludwig Gerlach, Iris Morr, Franz Oberdorfer, Gunnar Brix, Josef Doll, Johannes Blatter and Gerhard van Kaick

Department of Oncological Diagnostics and Therapy, German Cancer Research Center, Heidelberg, Germany; and Lilly Deutschland, Bad Homburg, Germany

This study was performed to investigate the effect of the new chemotherapeutic agent gemcitabine on glucose transport and metabolism in prostate carcinoma in vitro and in vivo. **Methods:** After transplantation of rat prostate adenocarcinoma cells, dynamic PET measurements with fluorine-18-labeled 2-fluoro-2-deoxy-D-glucose (^{18}FDG) were performed in 15 animals before and 1 day after therapy with 90 mg/kg of body weight (n = 8) and 180 mg/kg of body weight (n = 7) gemcitabine. In the second examination, the animals received a simultaneous injection of ^{18}FDG and [^{3}H]thymidine. Quantitative evaluation of the PET data was done using the standardized uptake value (SUV) as well as a three-compartment pharmacokinetic model. Furthermore, the incorporation of [^{3}H]thymidine into the DNA was determined. In vitro measurements of the FDG, 3-O-methylglucose and thymidine uptake were performed immediately and 4 hr after a 24-hr incubation period with different doses of gemcitabine. **Results:** FDG–SUV and the metabolic rate of FDG utilization did not change significantly after therapy. However, the values for the transport rate constants K_1 and k_2 increased significantly. The incorporation of thymidine into the DNA of treated tumors showed an 80% decline as compared with a control group. In the cell culture experiments, a dose-dependent increase of FDG (up to 178%) and 3-O-methylglucose uptake (up to 305%) was demonstrated. The thymidine uptake showed a 96% decline in the nucleic acid fraction and an increase of up to 337% in the cytoplasmic fraction. **Conclusion:** The more global measures of FDG metabolism as SUV and metabolic rate of FDG utilization were unchanged after therapy, while DNA synthesis and cell viability declined. However, in vitro and in vivo evidence of an enhancement of glucose transport is presented, indicating that quantification by modeling may be superior for the evaluation of metabolic effects during chemotherapy.

Key Words: fluorine-18-FDG; PET; gemcitabine; prostate adenocarcinoma; chemotherapy

J Nucl Med 1997; 38:1215–1221

Gemcitabine (2′,2′-difluoro-2′-deoxycytidine, dFdC) is a novel anticancer agent that must be metabolized in the cell into its active nucleotide forms. The drug is phosphorylized by deoxycytidine kinase, which is the rate-limiting enzyme for the formation of the active anticancer metabolites: dFdC diphosphate and dFdC triphosphate. dFdC diphosphate inhibits ribonucleotide reductase (*1*), the enzyme that produces deoxynucleotides required for DNA synthesis and repair. Subsequently, deoxycytidine triphosphate (dCTP) levels decrease, which is important because dFdC triphosphate competes with dCTP for incorporation into DNA by DNA polymerases (*2*). The decrease of the cellular concentration of dCTP results in an increase of the gemcitabine incorporation into the DNA, a self-potentiating mechanism. After the gemcitabine nucleotide is incorporated at the end of the elongating DNA strand, one more nucleotide is

Received Aug. 1, 1996; revision accepted Nov. 6, 1996.

For correspondence or reprints contact: Uwe Haberkorn, MD, Department of Oncological Diagnostics and Therapy, German Cancer Research Center, Im Neuenheimer Feld 280, D-69120 Heidelberg, Germany.

incorporated, and the DNA polymerases are unable to proceed. The drug is locked in the DNA, and proofreading enzymes are unable to remove the gemcitabine nucleotide from this position (masked chain termination).

PET with fluorine-18-labeled 2-fluoro-2-deoxy-D-glucose (^{18}FDG) allows quantitation of the metabolic state of malignant lesions. Therefore, the comparison of the values before and after therapy may be used for the early assessment of therapeutic efficacy (*3–7*). In this study, we investigated the effects of gemcitabine on the PET–FDG signal in prostate adenocarcinoma. Different PET quantitation procedures were evaluated and compared with cell culture studies using the same tumor model. Furthermore, thymidine uptake experiments were performed in vivo as well as in vitro to assess the effects of gemcitabine treatment on DNA synthesis.

MATERIALS AND METHODS

Animal Studies

The experiments were performed in compliance with German laws relating to the conduct of animal experimentation. Four × 10^6 tumor cells (Dunning R3327 rat prostate adenocarcinoma, subline AT1) were transplanted subcutaneously into the right thigh of male young adult Copenhagen rats (Olag, Blackthorn, U.K.). The PET measurements were performed 14–20 days later. Only animals with tumor diameters of more than 20 mm were accepted for the examination. After premedication with 50 mg/kg body weight (bw) ketamine and 0.5 mg/kg-bw *N*-(3′-dimethylaminopropyl)-3-propionyl-phenothiazine phosphate, the animals were kept in an inhalation narcosis with enflurane (0.4 volume-percent), nitrous oxide (flow 1000 ml/min) and oxygen (flow 500 ml/min) during the PET examination. Skin markings were performed at the site of the largest tumor diameter to ensure correct repositioning.

PET. The production of ^{18}FDG was done according to the method described by Oberdorfer et al. (*8*). The radiochemical purity was determined by high performance liquid chromatography (HPLC) with values above 98%. The PET studies were performed with a PC2048–7WB whole-body scanner. After administration of 12.5–25.0 MBq ^{18}FDG in a permanent catheter positioned in the jugular vein, the FDG uptake was measured dynamically over 90 min (acquisition frames: 12 × 5 sec, 6 × 10 sec, 6 × 30 sec, 5 × 60 sec, 6 × 300 sec and 5 × 600 sec). Immediately after this baseline measurement of FDG uptake, the animals (weighing 270–360 g) were treated by intravenous administration of 90 mg/kg-bw gemcitabine (Lilly GmbH, Bad Homburg, Germany) or 2 × 90 mg/kg-bw gemcitabine with the second dose after 12 hr. Since gemcitabine has a plasma half life of 68 min in rats, the second schedule was applied to maintain a more stable plasma level as well as to increase the dose of the drug. A follow-up FDG–PET examination was done with the same animals 24 hr after the onset of therapy. In this trial, we injected simultaneously 14.5–24.4 MBq ^{18}FDG and 3.7 MBq (*methyl*-[^{3}H])thymidine (specific activity 185 GBq/mmol, radioactive concentration 37 MBq/ml, radiochemical purity 97.5%). Before each PET study, the plasma glucose level (C_p) (in micromoles per gram) of the animals was determined using a commercially available kit.

Before the PET emission scanning, a 30-min blank scan and a 15-min transmission scan were performed using a ^{68}Ge rod source. The emission sinograms were subsequently corrected for scattered radiation (*9*) and attenuation (*10*) as described elsewhere. PET images with a slice thickness of 8 mm (cross plane) and 11 mm (direct planes) were generated by use of a maximum-likelihood reconstruction algorithm with overrelaxation for accelerated convergence (*11–13*) on a DEC 3000/400 AXP workstation. The image matrix was 256 × 256 with a pixel size of 2 × 2 mm at a spatial in-plane resolution of 5.1 mm.

For quantitative evaluation, regions-of-interest were defined in the medial portion ("hottest" area) of the tumors with region sizes exceeding 32 pixels in all cases. Time-activity curves were generated and corrected for radionuclide decay ($T_{1/2}$ = 109.7 min). Finally, FDG uptake was expressed as the standardized uptake value (SUV) according to

$$SUV = \frac{C}{D/m}, \qquad \text{Eq. 1}$$

with C the tissue activity concentration (in kBq per gram), D the injected dose (in kBq) and m the body weight (in grams).

Immediately after the second PET examination, the animals were killed, and the tumors were removed and weighed. Tumor samples from the medial portion were frozen in liquid nitrogen for further DNA extraction.

Pharmacokinetic Analysis. A three-compartment pharmacokinetic model, originally developed for the brain (*14,15*), was used for assessment of FDG transport and phosphorylation in the tumors. The ^{18}FDG concentration in the arterial blood plasma, the arterial input function, was determined in a separate study from six rats with an extracorporeal loop placed between the carotid artery and the jugular vein. After administration of 27.2–41.3 MBq ^{18}FDG into the jugular vein, the total ^{18}F activity concentration in the extracorporeal loop was measured continuously over 90 min using a BGO fluid monitor with a temporal resolution of 500 ms. At 5, 10, 30, 60 and 90 min after ^{18}FDG injection, blood samples (volume ≈100 μl) were taken from the extracorporeal loop. The ^{18}F radioactivity concentrations in the whole blood and plasma were determined with an automated NaI(Tl) well counter referenced to a 511-keV ^{68}Ga/^{68}Ge calibration standard. HPLC analysis of the plasma samples (*16,17*) showed only ^{18}FDG and no FDG metabolites in the arterial plasma. The measured ^{18}F time-activity profiles were calibrated using the whole blood samples, corrected for the FDG uptake in the red blood cells, and standardized to the injected radioactivity and the body weight. The arterial plasma data from the six animals were averaged to provide a reference arterial input function for the subsequent pharmacokinetic analysis.

The tracer kinetic model for analysis of the individual tumor time-activity curves consisted of three compartments with (a) FDG in arterial plasma, (b) FDG in tissue and (c) FDG-6-phosphate in tissue. The model configuration was realized within the ADAPT II program environment (*18*) on a DEC 3000/400 AXP workstation and included nonlinear least-squares fitting for parameter estimation. The rate constants that describe the compartmental fluxes include K_1 (in milliliters per minute per gram) and k_2 (in reciprocal minutes) for forward and backward transport of FDG, respectively. The rate constants k_3 (in reciprocal minutes) and k_4 (in reciprocal minutes) refer to the phosphorylation of FDG and the dephosphorylation of FDG-6-phosphate in the tumor tissue, respectively. The model configuration included two additional fit parameters: a vascular volume term V_p (in percent) to account for nonextracted FDG activity remaining within the tumor tissue vascular space and an input function time delay parameter T_d (in seconds) to correct for the time delay of ^{18}FDG activity arrival in the extracorporeal detector loop.

Since the lumped constant to account for the differences between glucose and FDG transport and phosphorylation (*15*) is unknown for the rat prostate adenocarcinoma, we restricted our analysis to the FDG metabolism. Hence, the metabolic rate of FDG utilization (MR_{FDG}) (in micromoles per minute per gram) was computed as described (*14,15*):

$$MR_{FDG} = \frac{C_p}{LC} * \frac{K_1 * k_3}{k_2 + k_3}, \qquad \text{Eq. 2}$$

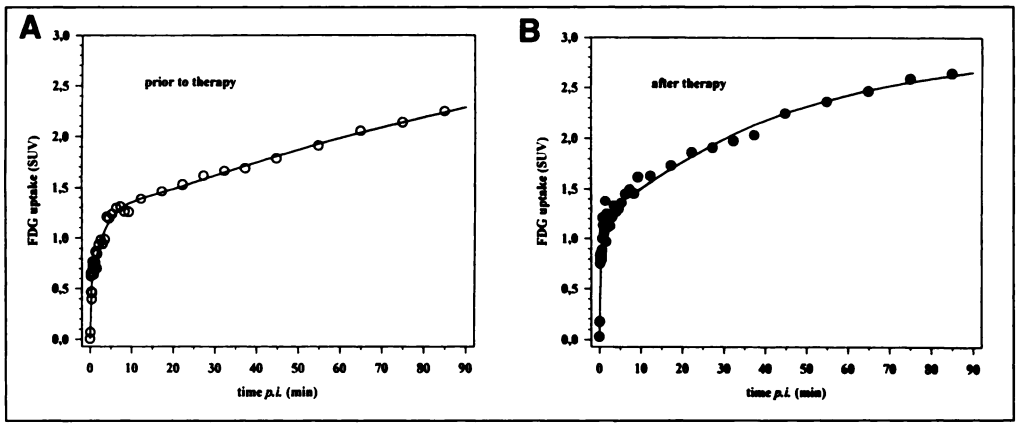

FIGURE 1. FDG uptake in a rat prostate adenocarcinoma before (A) and 24 hr after (B) administration of 180 mg/kg-bw genicitabine. Fit curve from pharmacokinetic analysis with a three-compartment model. Rate constants before therapy: K_1 = 0.037 ± 0.002 ml/min/g, k_2 = 0.12 ± 0.02 min^{-1} and k_3 = 0.05 ± 0.02 min^{-1}. Rate constants after therapy: K_1 = 0.060 ± 0.004 ml/min/g, k_2 = 0.31 ± 0.05 min^{-1} and k_3 = 0.12 ± 0.02 min^{-1}.

with C_p as the plasma glucose concentration (in micromoles per gram) and LC as the lumped constant with LC = 1.

DNA Extraction. Tumor pieces were minced and digested overnight at 55°C in 700 μl lysis buffer (100 m*M* NaCl, 10 m*M* Tris at pH 8, 25 m*M* EDTA at pH 8, 0.5% sodium dodecyl sulfate, and 0.1 mg/ml proteinase K). The lysates were then washed after addition of 3 ml phenol for 30 min and rotated at 3000 rpm in a Heraeus Minifuge for 10 min. The supernatant was washed with 3 ml of a phenol/chloroform-isoamylalcohol (CIA; ratio 24:1) mixture (ratio phenol/CIA 1:1) for 15 min. After centrifugation (10 min at 3000 rpm), the supernatant was washed with CIA for 15 min and rotated (10 min at 3000 rpm) to remove the remaining phenol. To the supernatant, 0.1 vol 3 *M* sodium acetate and 1 vol isopropanol were added to precipitate the DNA. After centrifugation, the pellet was washed with 70% ethanol and air dried. The pellet was resuspended in water and the DNA concentration was determined photometrically at 260 nm. Thereafter, the incorporated radioactivity was measured in a scintillation counter and normalized to the DNA content (in becquerels per milligram of DNA). The thymidine values of the treated animals were then compared to the thymidine incorporation determined in eight untreated animals.

In Vitro Studies

For all in vitro experiments, the same rat prostate adenocarcinoma cells (Dunning R3327 rat prostate adenocarcinoma, subline AT1) as used in the in vivo study were used. The cells were maintained in culture flasks in RPMI 1640 medium supplemented with 292 mg/liter glutamine, 100,000 IE/liter penicillin, 100 mg/liter streptomycin and 10% fetal calf serum at 37°C in an atmosphere of 95% air/5% CO_2. Each of the following experiments was done in triplicate.

The cells were trypsinized, and 5 × 10^4 cells were seeded in 6-well plates. One day later, the cells were treated with 10, 50 or 100 n*M* gemcitabine for 24 hr followed by the FDG, 3-O-methylglucose and thymidine uptake experiments.

FDG Uptake. The uptake experiments were performed immediately and 4 hr after the end of therapy in glucose-free RPMI 1640 medium supplemented with glutamine and penicillin/streptomycin. After 30 min of preincubation, 37 kBq 2-fluoro-2-deoxy-D-[U-^{14}C]glucose (FDG, specific activity 10.8 GBq/mmol, radioactive concentration 7.4 MBq/ml, radiochemical purity 99.3%) and cold FDG was added per milliliter of medium to a final concentration of 0.1 m*M*. After a 10-min incubation period, the medium was removed and the cells were washed twice with ice-cold phosphate buffered saline (PBS). The lysis was done on ice using ice-cold 0.6 *M* perchloric acid and a cell scraper. Thereafter, the lysates were neutralized with 1 *M* KOH and 0.5 *M* Tris/HCl (pH 7) and counted by scintillation counting. The measured radioactivity was standardized to the viable cell number as determined in parallel plates by a Coulter counter and trypan blue staining (more than 94% viable cells).

3-O-Methylglucose Uptake. After 30 min of preincubation, 185 kBq/ml 3-O-methyl-D-[^{3}H]glucose (specific activity 92.5 GBq/mmol, radioactive concentration 37 MBq/ml, radiochemical purity 99.5%) and cold 3-O-methylglucose in a final concentration of 0.05 m*M* were added. After a 10-min incubation period, the medium was removed and the cells were washed twice with ice-cold PBS. The lysis was done on ice using 0.3 *M* NaOH/10% sodium dodecyl sulfate and a cell scraper. Scintillation counting was performed as described above.

Thymidine Uptake. The cells were pulsed with 185 kBq (*methyl*-(*methyl*-[^{3}H])thymidine and cold thymidine in a final concentration of 0.05 m*M* for 2 hr in 1 ml medium. After removal of the medium, the cells were washed three times with ice-cold PBS. The lysis was performed with 0.5 *M* perchloric acid and a cell scraper. After 30 min on ice, the lysate was vortexed and rotated at 1500 × g for 5 min at 0°C. The supernatant was removed, and the pellets were washed with 0.5 *M* perchloric acid and rotated again for 5 min at 0°C. The pellet (= acid-insoluble fraction) was resuspended in 1 *M* NaOH at 37°C. Aliquots of the acid-insoluble and the acid-soluble (= both supernatants) fraction were taken for scintillation counting. The radioactivity was then expressed as pmol/10^5 cells.

RESULTS

Animal Studies

Eleven tumors were evaluable for the pharmacokinetic compartment analysis with median variation coefficients of 7% (K_1), 20% (k_2) and 18% (k_3). The plasma glucose levels were 121.8 ± 16.9 mg% and 120.8 ± 34.7 mg% before and after therapy, respectively. Figure 1 shows the fitting results for a tumor before (Fig. 1A) and 1 day after intravenous administration of 180 mg/kg-bw gemcitabine (Fig. 1B). After therapy, an increase in the transport and phosphorylation rate constants was observed although the SUV [at 90 min postinjection (p.i.)] was substantially unchanged. Furthermore, the FDG–SUV showed an increase during the whole examination period with no plateau reached even after 90 min.

In the 11 animals evaluable for the pharmacokinetic analysis, the metabolic rate and the SUV were correlated with r = 0.86 (significant at $p < 0.01$ (*19*); Fig. 2). The SUV decreased in 5/15 animals and increased in 8/15 animals, the rest being unchanged. A comparison of the different quantification procedures is shown in Figure 3. For the SUV and the metabolic rate no uniform changes were observed (Fig. 3A,B), whereas the kinetic rate constants for transport (Fig. 3C,D) and phosphorylation (Fig. 3E) were elevated in most cases. The pre- and post-therapeutic values were compared using a paired Student's t-test revealing no significant differences in SUV (p = 0.962),

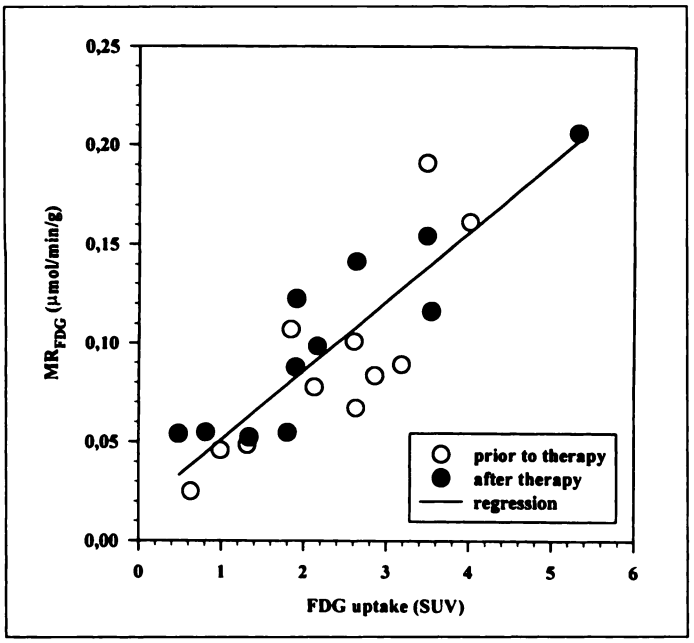

FIGURE 2. Comparison of the SUV obtained at 90 min p.i. and the metabolic rate constant of FDG utilization (MR_{FDG}) in 11 animals before and 24 hr after intravenous administration of gemcitabine.

MR_{FDG} ($p = 0.512$) and k_3 ($p = 0.156$) and significant differences for K_1 and k_2 (both $p < 0.01$).

The incorporation of tritiated thymidine into the DNA was decreased in the treated tumors as compared with the control group of untreated animals (n = 8): 126 ± 35 Bq/mg DNA in controls and 25.5 ± 12.8 Bq/mg DNA and 17.1 ± 15.1 Bq/mg DNA after treatment with 90 mg gemcitabine/kg-bw and 180 mg gemcitabine/kg-bw, respectively. The Student's t-test procedure revealed significant ($p < 0.01$) differences between controls and treated tumors. A significant difference of the thymidine incorporation into the DNA after 90 mg/kg-bw gemcitabine as compared with 180 mg/kg-bw gemcitabine was not found.

In Vitro Studies

The viable cell number declined to 32% and 23% of the controls after a dose of 10 n*M* and 100 n*M* gemcitabine, respectively (Fig. 4A). After a 2-hr pulse with tritiated thymidine, the radioactivity in the acid-insoluble fraction decreased in a dose-dependent manner to 4% of the controls (Fig. 4B). Simultaneously, the radioactivity in the acid-soluble fraction increased to 337% correct of the control rats (Fig. 4C). The increase in thymidine uptake was higher immediately after therapy than 4 hr after therapy.

Figure 5 shows the effects of gemcitabine on the FDG (Fig. 5A) and the 3-O-methylglucose (Fig. 5B) uptake. A standardization of the uptake values to the viable cell number revealed an increase of both tracers of up to 178% for FDG and of up to 305% for 3-O-methylglucose.

DISCUSSION

The principle of therapy monitoring with PET and FDG seems very simple: Therapy induced death of tumor cells leads to a decrease in tumor tracer uptake. Consequently, it has been proposed that FDG is a marker of tumor viability (*20*). Quantitation of the PET data is done mainly by two procedures. The normalization of the ^{18}FDG uptake to the applied dose and the body weight SUV is easily performed, and no arterial blood

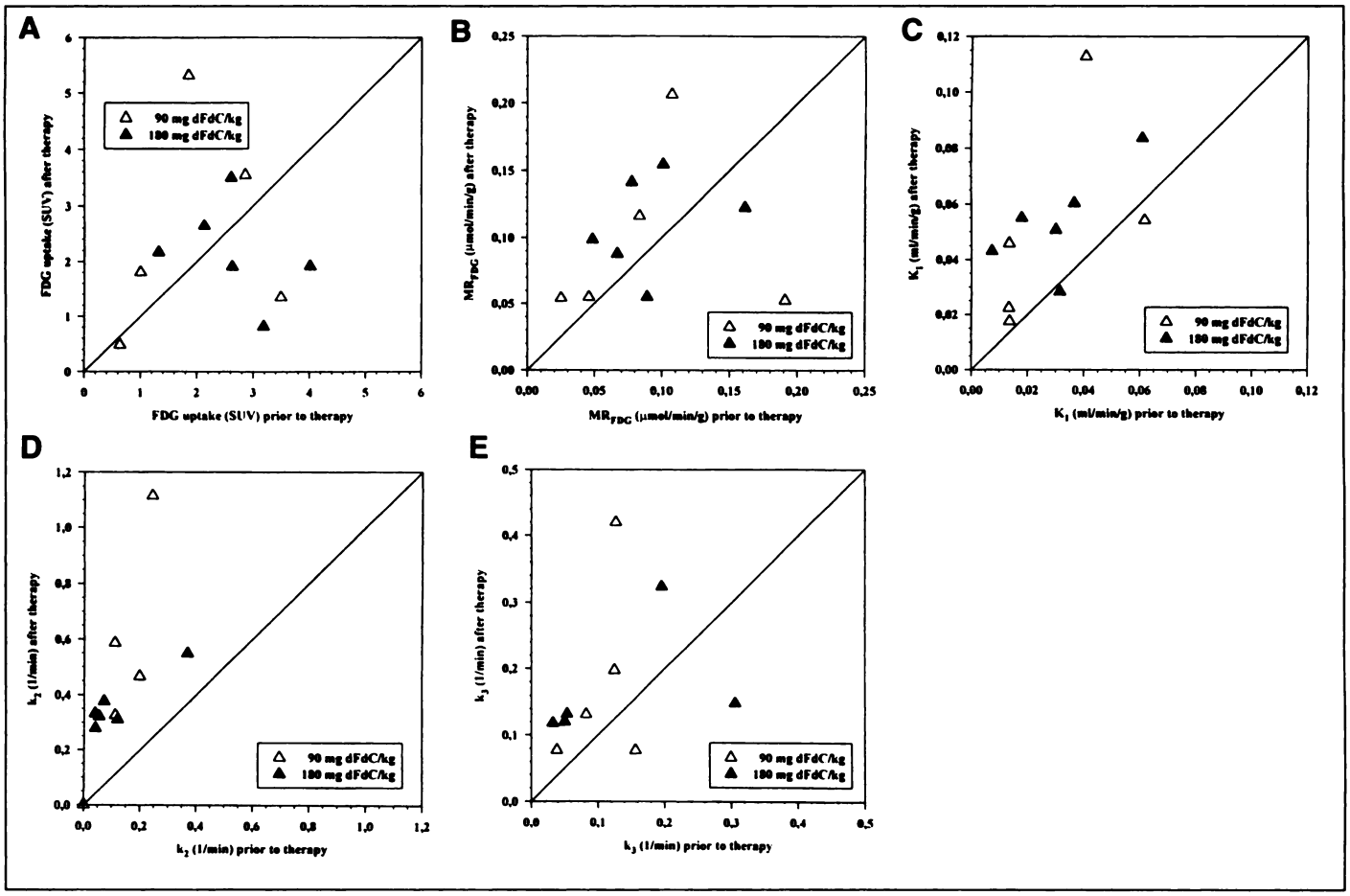

FIGURE 3. FDG uptake before and 24 hr after therapy with gemcitabine in 11 animals. Changes in SUV at 90 min p.i. (A), metabolic rate MR_{FDG} (B), forward transport rate K_1 (C), backward transport rate k_2 (D) and phosphorylation rate k_3 (E).

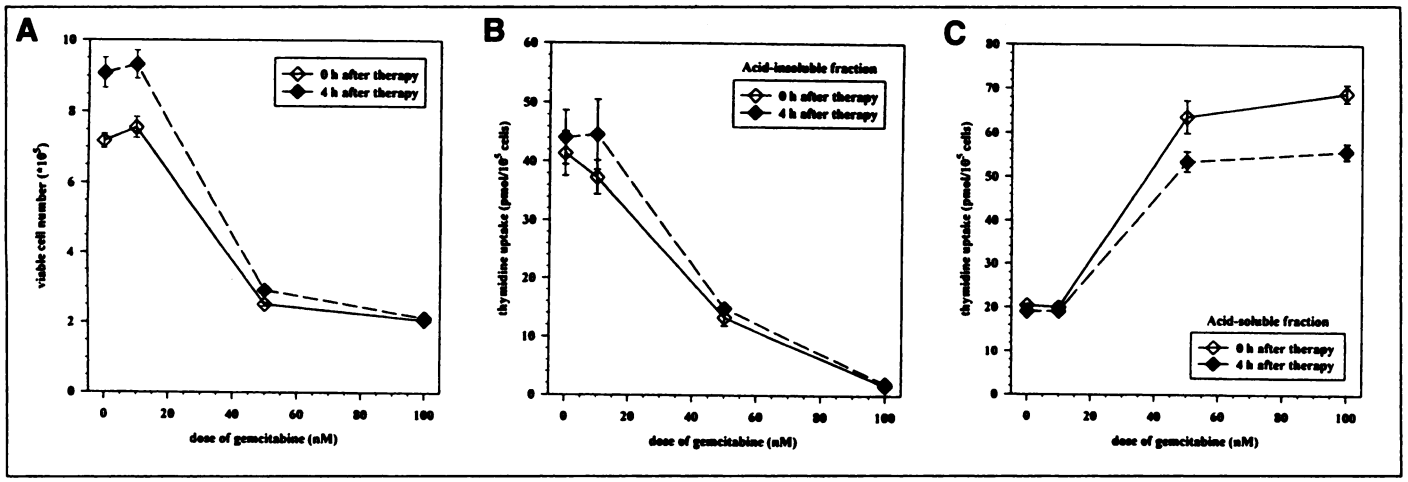

FIGURE 4. Viable cell number (A), thymidine uptake in the acid-insoluble (B) and the acid-soluble (C) fraction after perchloric acid extraction immediately and 4 hr after a 24-hr incubation period with different doses of gemcitabine. Mean values and s.d. are shown (n = 3).

sampling is needed. The SUV measured 50–90 min p.i. represents a combination of FDG transport and phosphorylation. However, the values obtained with this procedure are influenced by the patient body composition, the length of the uptake period, the plasma glucose level and partial volume effects (*21*). Furthermore, it is generally assumed that the FDG accumulation reaches a plateau after 60 min, and the SUV is usually calculated from the radioactivity extracted from a region of interest after this time period (*3–7*). However, our data show a steady increase even after 90 min in the rat prostate adenocarcinoma (Fig. 1).

The other procedure involves the application of a pharmacokinetic model, necessitating dynamic data of the tracer radioactivity in the arterial plasma to obtain the input function for the determination of transport and/or metabolic rate constants. These data are usually measured from discrete blood samples taken from an arterial catheter. Alternatively, the input function can be extracted from the PET images (*4*). In our study, we used an averaged arterial input function measured at high temporal resolution in six rats with an extracorporeal loop in an independent experiment. This averaged input function was found to be similar to an average input function, which was obtained in a separate study from six animals 1 day after treatment with gemcitabine (data not shown). Therefore, therapy with gemcitabine does not lead to changes in the input function in treated animals, and the average input function of the six untreated animals was used in all experiments.

Thymidine incorporation into the DNA was decreased in treated animals 1 day after drug application as compared with the control group, which provides evidence for the effectiveness of gemcitabine in this tumor model. Obviously, DNA synthesis is impaired in these tumors. However, no significant decrease in FDG uptake was observed. Differences in the FDG quality can be excluded, since a HPLC quality control is done routinely in our laboratory before the administration of FDG. Furthermore, varying partial volume effects due to incorrect repositioning in the PET experiment may explain the difference between the thymidine and the FDG data. However, skin markings were performed at the site of the largest tumor diameter to ensure correct repositioning, and a high resolution image reconstruction technique was used that intrinsically accounts for partial volume effects (*12*).

Our data show differing results for the two different quantitation procedures used: No uniform change of the SUV 90 min p.i. was observed (Fig. 3A). The same applies to the metabolic rate (Fig. 3B), which is highly correlated to the SUV (Fig. 2). However, the modeling analysis revealed a significant increase of the individual transport (K_1 and k_2) rate constants (Fig. 3C,D). Furthermore, the in vitro experiments showed an increase in FDG and 3-O-methylglucose uptake (Fig. 5). The increase of the transport tracer 3-O-methylglucose provides evidence for an enhancement of the glucose transport capacity. The congruency of the in vitro data with the results of the modeling analysis thus suggests that combined parameters such

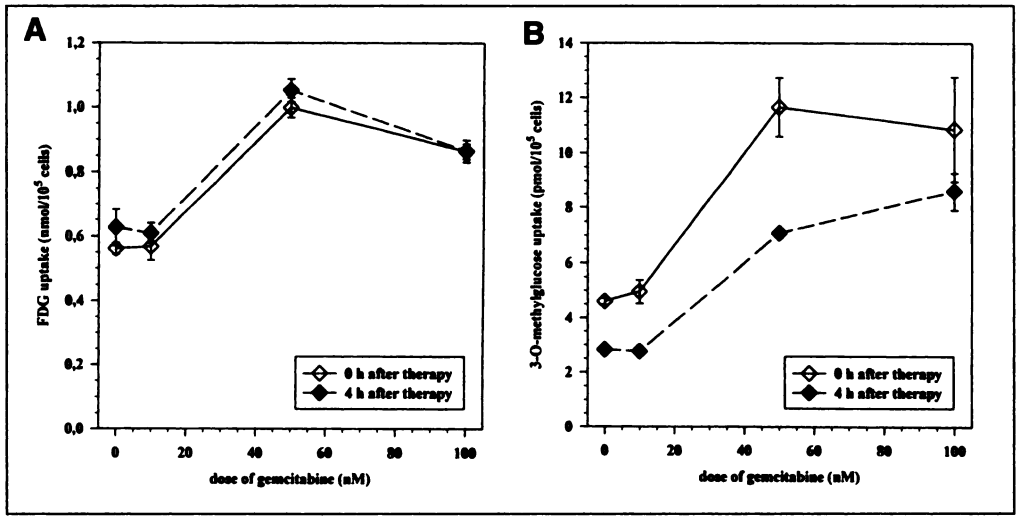

FIGURE 5. FDG uptake (A) and 3-O-methylglucose uptake (B) immediately and 4 hr after a 24-hr incubation period with different doses of gemcitabine. Mean values and s.d. are shown (n = 3).

as the SUV and the metabolic rate seem to be of limited value for the detailed assessment of the tumor's metabolic state as compared with the individual pharmacokinetic rate constants. However, it has to be mentioned that K_1 is also a composite parameter that includes delivery of the tracer (i.e., blood flow), capillary permeability, motion through the interstitial space and cellular transport. This may explain why k_2 was found to be greater than K_1 in our study with prostate adenocarcinoma as well as in studies of cerebral glucose metabolism (*14,15*), although tumor and brain tissue express predominantly the GLUT1 isoform of the glucose carrier, which shows a considerable kinetic asymmetry favoring influx (*22*).

The phenomenon of an enhanced glucose transport was observed in earlier studies with shorter exposure times to gemcitabine (*23*) and also after exposure of tumor cells with other chemotherapeutic agents (*16,17,24,25*) or after radiotherapy (*20*). In a clinical study, Rozenthal et al. found an increase of the regional cerebral metabolic rate in brain tumors after chemotherapy, which decreased to the baseline value during the following four days (*5*). Furthermore, an increase in glucose transport has been observed as a reaction to cellular stress. The glucose carrier shows a complex regulation: Glucose transport may be altered by phosphorylation of the transport protein (*26*), decreased degradation (*27*), translocation from intracellular pools to the plasma membrane (*28–30*) or an increased expression of the gene (*31*). The increase in glucose transport after exposure of cells to damaging agents has been ascribed mainly to a redistribution of the glucose transport protein from intracellular pools to the plasma membrane. Such reactions have been found in cells exposed to arsenite, calcium ionophore A23187 or 2-mercaptoethanol (*28–30,32,33*).

In a recent study with the same tumor cells, we also found evidence for a translocation of the glucose transporter after a shorter incubation time with gemcitabine (*23*). According to these findings, the post-therapeutic FDG signal is a result of several intratumoral changes: death of tumor cells leads to a decreased FDG accumulation. However, immune reactions may be induced, and the invasion of immune competent cells may elevate the FDG uptake. Furthermore, stressed tumor cells show an enhancement of glucose transport. These phenomena may compensate for the decreased uptake caused by tumor cell death and even lead to an increase in FDG uptake. This complex situation may depend on the tumor type as well as the therapy applied—e.g., it may last some days for brain tumors during chemotherapy (*5*) or several months for colorectal tumors after radiotherapy (*7*). Therapy monitoring with FDG seems to be of limited value during this time interval. Therefore, multi-tracer studies using markers of proliferation (such as [^{11}C]thymidine) or protein synthesis (such as [^{18}]fluorotyrosine) may lead to a better characterization of the biological state of a treated tumor.

In vitro, the incorporation of thymidine into the DNA decreased, whereas the radioactivity in the acid-soluble fraction, i.e., the nonincorporated or metabolized thymidine, increased (Fig. 4). This finding has also been observed in osteosarcoma cells after treatment with cisplatin and may be explained by an increase of the salvage pathway, e.g., of thymidine kinase activity (*17*). For this reason, the thymidine uptake in treated cells is not necessarily caused by thymidine incorporation into the DNA. Although [^{11}C]thymidine has been suggested as a proliferation marker for PET measurements (*34,35*), the assumption that during or after therapy all of the activity is incorporated into the DNA leads to an overestimation of the proliferative activity in the tumor cells. Therefore, it is unlikely that a quantification of the [^{11}C]thymidine accumulation by use of the SUV is successful for the determination of the proliferation in treated tumors.

PET with [^{11}C]thymidine measures the total radioactivity in a given tissue volume. The interpretation of these values requires information about thymidine metabolism and the size of the different metabolite fractions, which may be delivered by a modeling approach. However, this approach is complicated by the fact that multiple metabolites of thymidine occur that necessitate multiple HPLC analyses of the blood plasma (*36,37*). The choice of the carbon-2 as labeling position instead of the methyl group provides an advantage in this respect by reducing the number of possible metabolites (*38*) but does not eliminate the problem. Therefore, nucleoside analogs such as 5-fluoro-1-(2′-deoxy-2′-fluoro-β-D-ribofuranosyl)uracil may be better candidates for the measurement of tumor proliferation (*39*).

CONCLUSION

Gemcitabine induces a decrease in thymidine incorporation into the DNA and an enhancement of glucose transport in rat prostate adenocarcinoma shortly after treatment. These phenomena can be measured with PET and appropriate radioactive tracers like ^{18}FDG or [^{11}C]thymidine. However, early changes in tumor metabolism may be missed by a quantitation using the SUV. In contrast, the application of a pharmacokinetic model delivers more detailed information about the metabolic state of treated tumors, which is evidenced by the congruency of the in vivo and the in vitro data. Therefore, dynamic measurements and pharmacokinetic modeling may be superior at least at this early stage after therapy.

ACKNOWLEDGMENTS

We thank E. Bender, W. Konowalczyk, H. Marx, A. Theobald, H. Trojan, U. Wagner, K. Weber and W. Weber for their help in performing this study.

REFERENCES

1. Gandhi V, Plunkett W. Modulatory activity of 2′,2′-difluorodeoxycytidine on the phosphorylation and cytotoxicity of arabinosyl nucleosides. *Cancer Res* 1990;50: 3675–3680.
2. Grunewald R, Kantarjian H, Keating MJ, Abbruzzese J, Tarasoff P, Plunkett W. Pharmacologically directed design of the dose rate and schedule of 2′,2′-difluorodeoxycytidine (gemcitabine) administration in leukemia. *Cancer Res* 1990;50:6823–6826.
3. Minn H, Paul R, Ahonen A. Evaluation of treatment response to radiotherapy in head and neck cancer with fluorine-18 fluorodeoxyglucose. *J Nucl Med* 1988;29:1521–1525.
4. Wahl RL, Zasadny K, Helvie M, Hutchins GD, Weber B, Cody R. Metabolic monitoring of breast cancer chemohormonotherapy using positron emission tomography: initial evaluation. *J Clin Oncol* 1993;11:2101–2111.
5. Rozenthal JM, Levine RL, Nickles RJ, Dobkin JA. Glucose uptake by gliomas after treatment. *Arch Neurol* 1989;46:1302–1307.
6. Haberkorn U, Strauss LG, Dimitrakopoulou A, et al. Fluorodeoxyglucose imaging of advanced head and neck cancer after chemotherapy. *J Nucl Med* 1993;34:12–17.
7. Haberkorn U, Strauss LG, Dimitrakopoulou A, et al. PET studies of fluorodeoxyglucose metabolism in patients with recurrent colorectal tumors receiving radiotherapy. *J Nucl Med* 1991;32:1485–1490.
8. Oberdorfer F, Hull WE, Traving BC, Maier-Borst W. Synthesis and purification of 2-deoxy-2-^{18}fluoro-D-glucose and 2-deoxy-2-^{18}fluoro-D-mannose: characterization of products by ^{1}H and ^{19}F-NMR spectroscopy. *Int J Appl Radiat Isot* 1986;37:695–701.
9. Hoverath H, Kübler WK, Ostertag HJ, et al. Scatter correction in the transaxial slices of a whole-body positron emission tomograph. *Phys Med Biol* 1993;38:717–728.
10. Ostertag H, Kübler WK, Doll J, Lorenz WJ. Measured attenuation correction methods. *Eur J Nucl Med* 1989;15:722–726.
11. Bellemann ME, Doll J, Brix G, et al. PET image reconstruction for pharmacokinetic modeling of 5-[^{18}F]fluorouracil in liver tumors. In: Bergmann H, Sinzinger H, eds. *Radioactive Isotopes in Clinical Medicine and Research.* Basel, Switzerland: Birkhäuser; 1995:79–84.
12. Brix G, Doll J, Bellemann ME, et al. Use of scanner characteristics in iterative image reconstruction for high-resolution PET studies of small animals. *Eur Nucl Med* 1997: in press.
13. Shepp LA, Vardi Y. Maximum likelihood reconstruction for emission tomography. *IEEE Trans Med Imaging* 1982;1:113–122.
14. Phelps ME, Huang SC, Hoffman EJ, Selin C, Sokoloff L, Kuhl DE. Tomographic measurement of local cerebral glucose metabolic rate in humans with (F-18)2-fluoro-2-deoxy-D-glucose: validation of method. *Ann Neurol* 1979;6:371–388.

15. Huang SC, Phelps ME, Hoffman EJ, Sideris K, Selin CJ, Kuhl DE. Noninvasive determination of local cerebral metabolic rate of glucose in man. *Am J Physiol* 1980;238:E69–E82.
16. Haberkorn U, Reinhardt M, Strauss LG, et al. Metabolic design of combination therapy: use of enhanced fluorodeoxyglucose uptake caused by chemotherapy. *J Nucl Med* 1992;33:1981–1987.
17. Haberkorn U, Oberdorfer F, Klenner T, et al. Metabolic and transcriptional changes in osteosarcoma cells treated with chemotherapeutic drugs. *Nucl Med Biol* 1994;21:835–845.
18. D'Argenio DZ, Schumitzky A. *ADAPT II User's Guide*. Los Angeles: Biomedical Simulation Resource, University of Southern California; 1992.
19. Sachs L. *Angewandte Statistik*. Berlin: Springer; 1984: 329–333.
20. Higashi K, Clavo AC, Wahl R. In vitro assessment of 2-fluoro-2-deoxy-D-glucose, L-methionine and thymidine as agents to monitor the early response of a human adenocarcinoma cell line to radiotherapy. *J Nucl Med* 1993;34:773–779.
21. Keyes JW. SUV: standardized uptake or silly useless value? *J Nucl Med* 1995;36: 1836–1839.
22. Lacko L, Wittke B, Kromphardt H. Kinetics of glucose uptake in erythrocytes: effect of trans-concentration. *Eur J Biochem* 1972;25:447–454.
23. Haberkorn U, Morr I, Oberdorfer F, et al. Fluorodeoxyglucose uptake in vitro: aspects of method and effects of treatment with gemcitabine. *J Nucl Med* 1994;35:1842–1850.
24. Slosman DO, Pugin J. Lack of correlation between tritiated deoxyglucose, thallium-201 and technetium-99m-MIBI cell incorporation under various cell stresses. *Eur J Nucl Med* 1994;35:120–126.
25. Minn H, Kangas L, Kellokumpu-Lehtinen P, et al. Uptake of 2-fluoro-2-deoxy-D-(U-^{14}C)-glucose during chemotherapy in murine Lewis lung tumor. *Nucl Med Biol* 1992;19:55–63.
26. Hayes N, Biswas C, Strout V, Berger J. Activation by protein synthesis inhibitors of glucose transport into L6 muscle cells. *Biochem Biophys Res Commun* 1993;190:881–887.
27. Shawver LK, Olson SA, White MK, Weber MJ. Degradation and biosynthesis of the glucose transporter protein in chicken embryo fibroblasts transformed by the src oncogene. *Mol Cell Biol* 1987;7:2112–2118.
28. Widnell CC, Baldwin SA, Davies A, Martin S, Pasternak CA. Cellular stress induces a redistribution of the glucose transporter. *FASEB J* 1990;4:1634–1637.
29. Pasternak CA, Aiyathurai JEJ, Makinde V. Regulation of glucose uptake by stressed cells. *J Cell Physiol* 1991;149:324–331.
30. Clancy BM, Czech MP. Hexose transport stimulation and membrane redistribution of glucose transporter isoforms in response to cholera toxin, dibutyryl cyclic AMP and insulin in 3T3 adipocytes. *J Biol Chem* 1990;265:12434–12443.
31. Flier JS, Mueckler MM, Usher P, Lodish HF. Elevated levels of glucose transport and transporter messenger RNA are induced by ras or src oncogenes. *Science* 1987;235: 1492–1495.
32. Hughes CS, Shen JW, Subjeck JR. Resistance to etoposide induced by three glucose-regulated stresses in Chinese hamster ovary cells. *Cancer Res* 1989;49:4452 4454.
33. Wertheimer E, Sasson S, Cerasi E, Ben-Neriah Y. The ubiquitous glucose transporter GLUT-1 belongs to the glucose-regulated protein family of stress-inducible proteins. *Proc Natl Acad Sci USA* 1991;88:2525–2529.
34. Christman D, Crawford EJ, Friedkin M, Wolf AP. Detection of DNA synthesis in intact organisms with positron-emitting (methyl-^{11}C)thymidine. *Proc Natl Acad Sci USA* 1972;69:988–992.
35. Poupeye EM, Goethals PP, Dams RF, De Leenheer AP, van Eijkeren ME. Evaluation of (^{11}C)thymidine for measurement of cell proliferation in fast dividing tissues. *Nucl Med Biol* 1993;20:359–362.
36. Shields AF, Coonrod DV, Quackenbush RC, Crowley JJ. Cellular sources of thymidine nucleotides: studies for PET. *J Nucl Med* 1987;28:1435–1440.
37. Shields AF, Lim K, Grierson J, Link J, Krohn KA. Utilization of labeled thymidine in DNA synthesis: studies for PET. *J Nucl Med* 1990;31:337–342.
38. Vander Borght TM, Lambotte LE, Pauwels SA, Dive CC. Uptake of thymidine labeled on carbon 2: a potential index of liver regeneration by positron emission tomography. *Hepatology* 1990;12:113–118.
39. Shields AF, Grierson JR, Kozawa SM, Zheng M. Development of labeled thymidine analogs for imaging tumor proliferation. *Nucl Med Biol* 1996;23:17–22.

Localization of Iodine-125-mIP-Des-Met^{14}-Bombesin (7-13)NH_2 in Ovarian Carcinoma Induced to Express the Gastrin Releasing Peptide Receptor by Adenoviral Vector-Mediated Gene Transfer

Buck E. Rogers, Maryland E. Rosenfeld, M.B. Khazaeli, Galina Mikheeva, Murray A. Stackhouse, Tiepu Liu, David T. Curiel and Donald J. Buchsbaum

Departments of Radiation Oncology, Medicine, and Gene Therapy Program, Comprehensive Cancer Center, University of Alabama at Birmingham, Birmingham, Alabama

The gastrin releasing peptide receptor (GRPr) has a high affinity for the 14 amino acid bombesin peptide. For this analysis, [^{125}I]-Tyr^4-bombesin was compared with [^{125}I]-mIP-bombesin (a seven amino acid bombesin analog) for in vitro binding and internalization into tumor cells and for tumor localization in vivo. Also, a recombinant adenoviral vector (AdCMVGRPr) was used for gene transfer to induce the expression of GRPr in human ovarian cancer cells for binding and tumor localization with these radiolabeled peptides. **Methods:** [^{125}I]-mIP-bombesin was synthesized and compared with [^{125}I]-Tyr^4-bombesin in internalization assays using BNR-11 cells (mouse fibroblast cells stably transfected with GRPr) over a 24-hr period. In vitro binding assays used BNR-11, and A427, HeLa and SKOV3.ip1 human cancer cells, which were either uninfected or infected with AdCMVGRPr. Biodistribution studies were performed in normal BALB/c mice and in athymic nude mice bearing orthotopic SKOV3.ip1 ovarian cancer tumors. The SKOV3.ip1 tumors were induced to express GRPr with the AdCMVGRPr adenoviral vector. **Results:** Internalization assays showed that [^{125}I]-Tyr^4-bombesin was rapidly internalized and catabolized at 37°C with ≈10% of the radioactivity remaining intracellularly at 4 hr, compared with ≈30% with [^{125}I]-mIP-bombesin. HeLa, A427 and SKOV3.ip1 cells were all induced to express levels of GRPr that were higher than those seen with the positive control BNR-11 cells. Normal mice showed a lower level of radioactivity in both the blood and thyroid for [^{125}I]-mIP-bombesin [0.26% ± 0.10% injected dose per gram (ID/g) and 0.24% ± 0.05% ID] than for [^{125}I]-Tyr^4-bombesin (3.5% ± 1.6% ID/g and 5.2% ± 4.4% ID) at 4 hr postinjection. Mice bearing intraperitoneal (i.p.) SKOV3.ip1 tumors and given AdCMVGRPr i.p. 5 days after tumor cell inoculation followed by [^{125}I]-mIP-bombesin i.p. at day 7 showed 16.5% ± 4.8% ID/g in tumor compared with 5.9% ± 3.0% ID/g with [^{125}I]-Tyr^4-bombesin at 4 hr postinjection. Tumor bearing mice given saline or a control adenovirus expressing the β-galactosidase (LacZ) gene showed significantly lower tumor uptake values of both bombesin peptides. **Conclusion:** Internalization assays showed that [^{125}I]-mIP-bombesin has favorable characteristics compared with [^{125}I]-Tyr^4-bombesin with regards to cellular internalization and retention. The results demonstrate successful in vitro and in vivo transduction of human tumor cells with a recombinant adenoviral vector-expressing GRPr. Additionally, tumors transduced in vivo to express GRPr demonstrated significantly greater localization of [^{125}I]-mIP-bombesin when compared with [^{125}I]-Tyr^4-bombesin.

Key Words: bombesin; gastrin releasing peptide receptor; adenovirus; gene transfer; iodine-125

J Nucl Med 1997; 38:1221–1229

Received Aug. 20, 1996; revision accepted Nov. 13, 1996.

For correspondence or reprints contact: Donald J. Buchsbaum, PhD, Department of Radiation Oncology, University of Alabama at Birmingham, 1824 6th Avenue South, Birmingham, AL 35294.